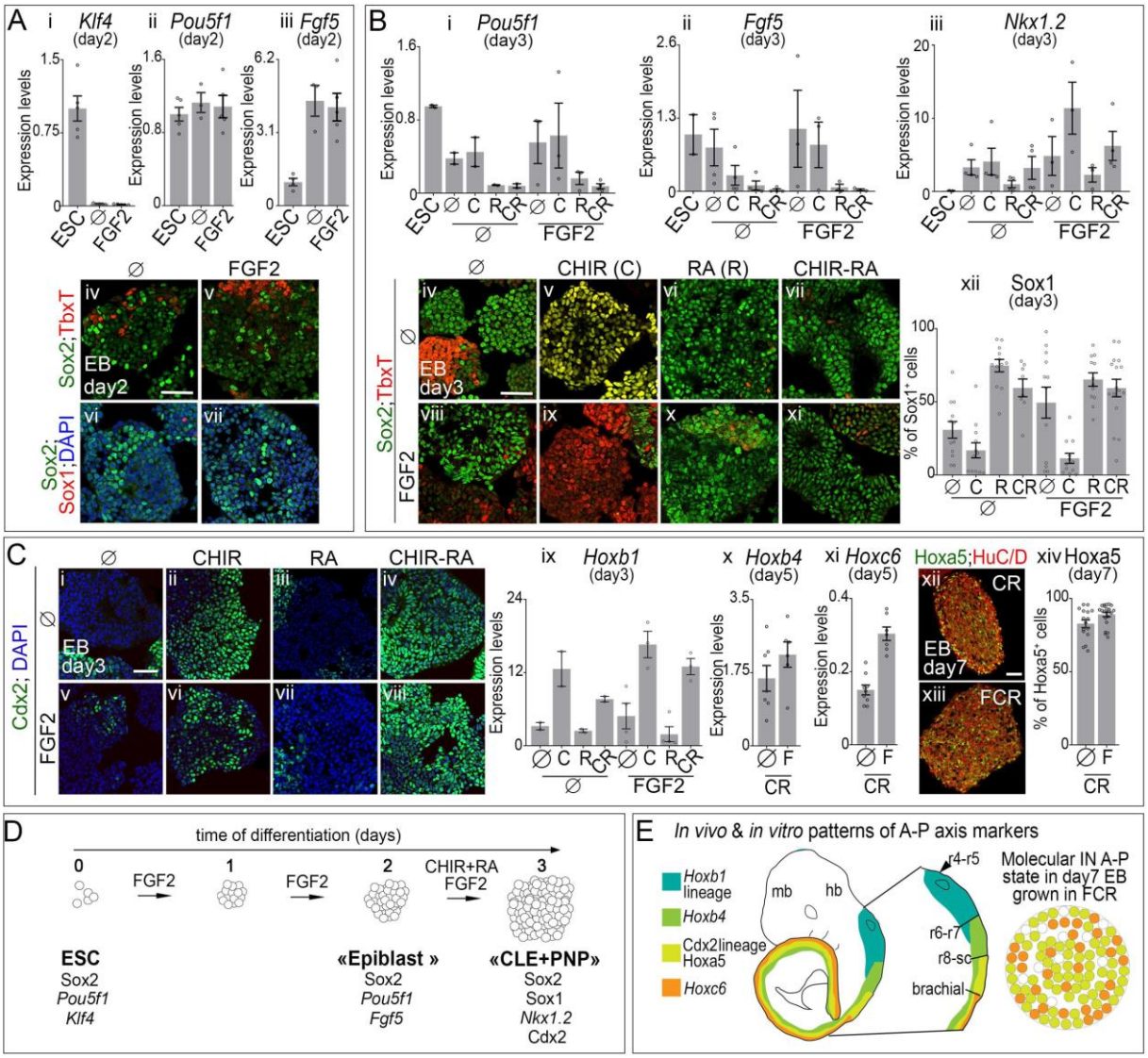

Fig. S1: FGF2, CHIR and RA impact on neural and caudal states of mouse ESC derived EB

(A)(Ai-iii) Levels of pluripotency markers *Klf4*, *Pou5f1* (*Oct4*), and *Fgf5* expression in ESC or in EB on their 2nd day of differentiation grown without any supplementation (∅) or with FGF2, quantified by RT-qPCR relative to *TBP* and normalized to their levels in ESC (circles: individual values, bars: mean±s.e.m.). **(Aiv-vii)** DAPI labelling and immuno-detection of TbxT, Sox2, and Sox1 in EB after two days in the indicated media. Scale bar: 60µM. By the 2nd day of differentiation, EB cells lost their *Pou5f1*$^{+}$;*Klf4*$^{+}$ pluripotency state, acquired epiblast molecular traits *(Pou5f1*$^{+}$;*Fgf5*$^{+}$;Sox2^{+}*)* and barely expressed specific lineage markers, such as Sox1 (neural) and TbxT (mesodermal).

(B) (Bi-iii) Expression levels of *Pou5f1*, *Fgf5* and *Nkx1.2* in ESC or in EB on their 3rd day of differentiation quantified by RT-qPCR relative to *TBP* and normalized to their levels in ESC in i and to levels in the tail bud of mouse embryos at gestational day (G.D.) 8.5 in ii and iii (circles: individual values, bars: mean±s.e.m.). **(Biv-xi)** DAPI labelling and immuno-detection of TbxT and Sox2 in EB after three days in the indicated media. Scale bar: 60µM. **(Bxii)** Quantification of $Sox1^+$ cells grown in the indicated media at day 3 (circles: individual values, bars: mean±s.e.m.). RA promoted the transition from an epiblast state to a neural state ($Sox1^+$; $Sox2^+$) and inhibited the synergic induction of the mesodermal marker TbxT by FGF2 and CHIR. Cells which are not differentiated may harbour a *Nkx1.2*$^+$ CLE state. These results are in line with several studies looking into the role of FGF and Wnt signalling during the establishment of caudal epiblast state (Beccari et al., 2018; Henrique et al., 2015).

(C)(Ci-viii) DAPI staining and immuno-detection of Cdx2 after 3 days of differentiation in the indicated media. Scale bar: 60µM**. (Cix,x,xiv)** Levels of *Hoxb1*, *Hoxb4* and *Hoxc6* quantified by RT-qPCR, relative to *TBP* expression and normalized to their levels in the spinal cord of G.D.11.5 mouse embryos in the indicated media and at the indicated stage of differentiation (circles: individual values, bars: mean±s.e.m.). **(Cxi-xiii)** Immuno-detection of Hoxa5 and HuC/D in the indicated conditions at day7 and quantification of the percentage of $Hoxa5^+$ cells per image field (circles: individual values, bars: mean±s.e.m.; scale bar: 60µM). C, R, F stand for CHIR, RA and FGF2, respectively.

CHIR triggered the caudalization of cells marked by the combined induction of Cdx2, *Hoxb1*, *Hoxb4*, Hoxa5 and *Hoxc6*, FGF2 increased *Hoxc6* expression. The molecular identities displayed by cells during the course of their differentiation [$Cdx2^+$ at day3, *Hoxb4*$^+$;*Hoxc6*$^+$ at day5 and $Hoxa5^+$ at day 7] in presence of FGF2, CHIR and RA indicate that they are driven towards a cervical-brachial state (Britz et al., 2015; Dasen et al., 2005). This is consistent with previous work demonstrating that FGF signalling is sufficient to caudalize the nervous system (e.g. (Liu et al., 2001).

(D) Schematics showing the state transitions of EB cells grown in presence of FGF2 between day0 and 3, CHIR and RA between day 2 and 3.

(E) Schematics showing the expression profiles of *Hoxb4*, *Hoxa5* and of *Hoxc6*, as well as the position of cells that had have expressed *Hoxb1* and Cdx2 in GD9.5 mouse embryos. Representation of day 7 EB grown in presence of FGF2 between day 0 and 3, CHIR and RA between day 2 and 3 inferred from data presented in C. Cells in EB grown in these conditions harboured an antero-posterior (A-P) state reminiscent of that found at the cervical-brachial levels of embryos.

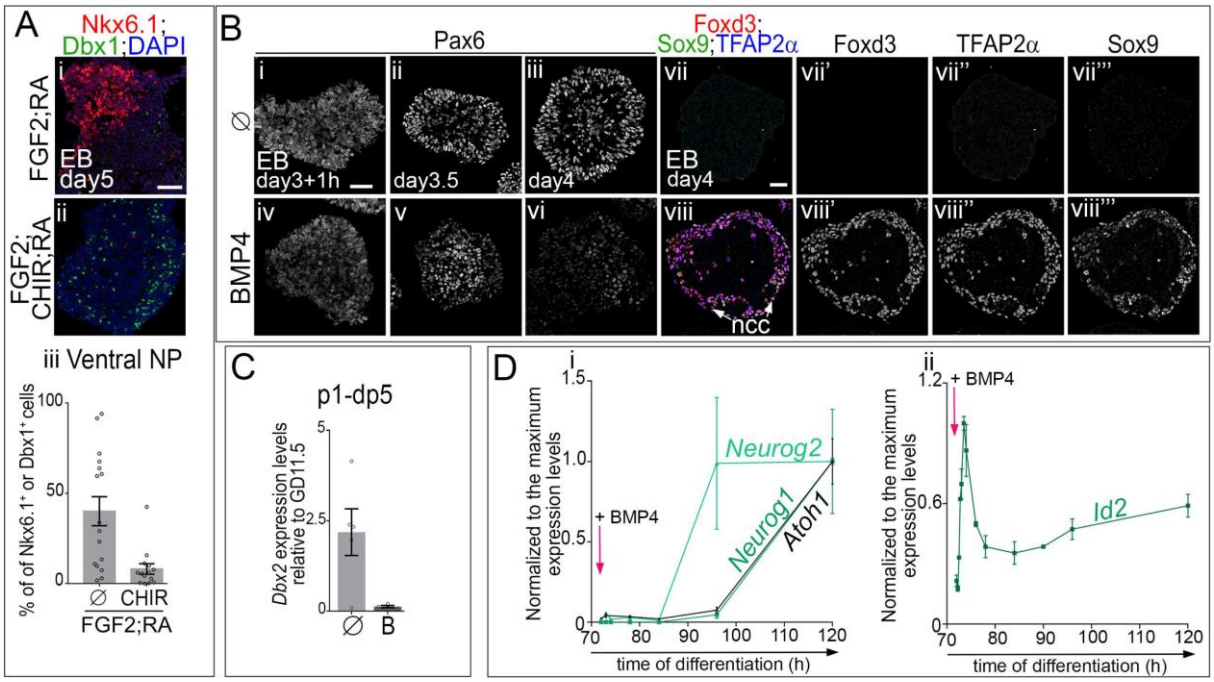

Fig. S2: Temporal and spatial dynamics in NP markers expression within dorsal spinal organoids

(A) Immuno-detection of Nkx6.1 and Dbx1 and DAPI labelling on day 5 EB cultured with FGF2 and RA with (ii) or without (i) CHIR (scale bar: 60µM) and quantification of the proportion of cells expressing either Nkx6.1 or Dbx1 per image field (circles: individual values, bars: mean±s.e.m.). CHIR mediated Wnt signalling activation dorsalised the states of NP in mouse derived EB, as shown by Nkx6.1 downregulation when CHIR is introduced in the culture medium.

(B-C) Immuno-detection of Pax6 or TFAP2β, Sox9, Foxd3 and DAPI labelling on EB at the indicated stages (B; scale bars: 60µM) and expression levels of *Dbx2*, a p1 to dp5 progenitor marker, assessed by RT-qPCR and normalized to its expression levels in G.D.11.5 mouse spinal cord in day5 EB (C). In these experiments EB were grown with FGF2, CHIR and RA without (Ø) or with (B) 5ng.ml^{-1} of BMP4 between day 3 and 4 of culture. Without BMP4 Pax6 expression increased between day3 and day3.5 suggesting that NP have acquired a new differentiated state; this could underpin the loss in the ability of cells to acquire a ncc state upon BMP4 exposure from day3.5 (i-iii, see Fig. 4B). In presence of BMP4, Pax6 levels decreased at the periphery of the EB as soon as 12hour post BMP4 addition (12hpa of BMP4), which is in agreement with cells acquiring a more dorsal fate (iv-vi, see Fig. 1A). In presence of BMP4 on day3 of differentiation cells at the periphery of the EB adopted a TFAP2β^{+};Foxd3^{+}; Sox9^{+}

ncc fate on day4, the presence of Foxd3 excluded the possibility that these cells were reminiscent to the pre-placodal ectodermal cells (Moody and LaMantia, 2015). The intermediate dorsal spinal cord marker *Dbx2* was present in day5 EB grown in absence of BMP4 which is in agreement with most EB cells that have adopted a dp4-dp6 fate. Its expression decreased upon BMP4 treatment.

(D) Expression levels of *Neurog2* (pale green line in i), *Neurog1* (dark green line in i), *Atoh1* (black line in i) and *Id2* (ii) assessed by RT-qPCR from day 3 to day 5 in EB cultured as in Fig. 1A with BMP4. In presence of BMP4, cells first induced the dp2/dp3 marker *Neurog2* before expressing the dp1 and dp2 markers *Atoh1* and *Neurog1*. This temporal sequence is similar to that found in vivo in cells that will acquire a dp1 state (Tozer et al., 2013). The temporal profile of BMP signalling target *Id2* confirmed that intracellular BMP signalling progressively decreased as soon as 1h after BMP4 addition (Samanta and Kessler, 2004; Hollnagel et al., 1999).

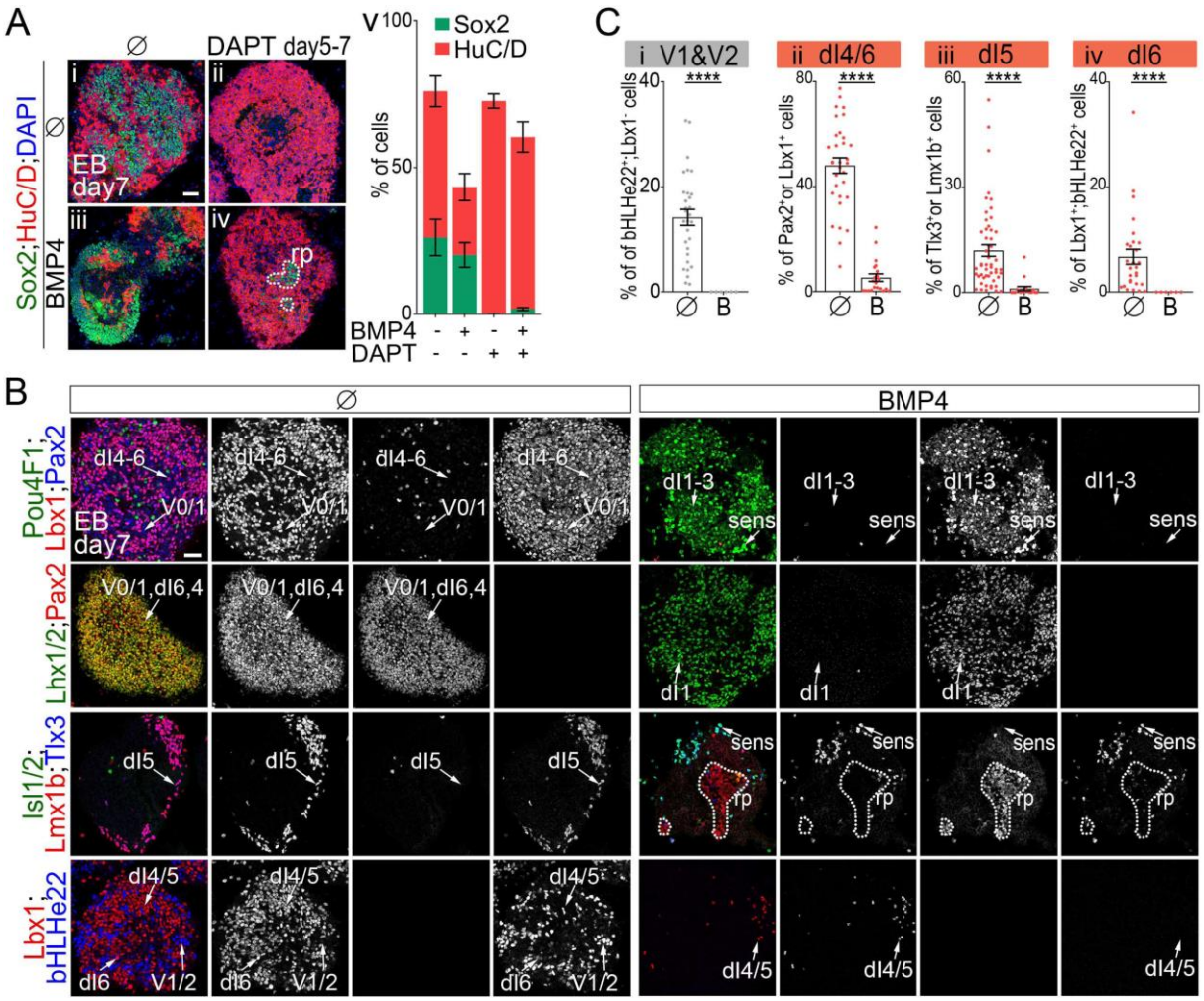

Fig. S3: Temporal and spatial dynamics in PM markers expression within dorsal spinal organoids

(A) Immuno-detection of Sox2 and HuC/D and DAPI labelling on day 7 EB cultured as in Fig. 1A treated with or without DAPT and with or without BMP4 (i-iv, scale bar: 60µM). Percentage of HuC/D$^+$ (red) and Sox2$^+$ (green) cells in day 7 mouse ESC derived EB grown in the indicated conditions (mean±s.e.m.). (v) BMP4 decreased the rate of differentiation of NP in EB. DAPT treatment from day 5 pushed BMP4 treated or not treated cells towards a terminally differentiated HuC/D$^+$ state.

(B) Immuno-detection of the indicated IN subtype markers on day 7 organoids treated or not with BMP4. Dash lines surround rp territory (scale bar: 60µM). **(C)** Percentage of ventral and associating IN subtypes harbouring the indicated TF code per image field (circles: individual values, bars: mean±s.e.m.). In absence of BMP4, the vast majority of cells within the organoid harboured a molecular identity reminiscent of one of the three major classes of early born associating neurons. It included 5% of Lbx1$^+$;bHLHe22$^+$ dI6 cells, 12% of Lbx1$^+$; Pou4f1$^+$ or Tlx3$^+$;Lmx1b$^+$ peripheral dI5 cells, and 45% of Lbx1$^+$;Pax2$^+$;bHLHe22$^-$ like cells. The remaining 20% of cells displayed a ventral V2 to V0 IN states. In presence of BMP4 these cell-types were no longer produced in the EB. Instead, a variety of dorsal cells were present in the organoids.

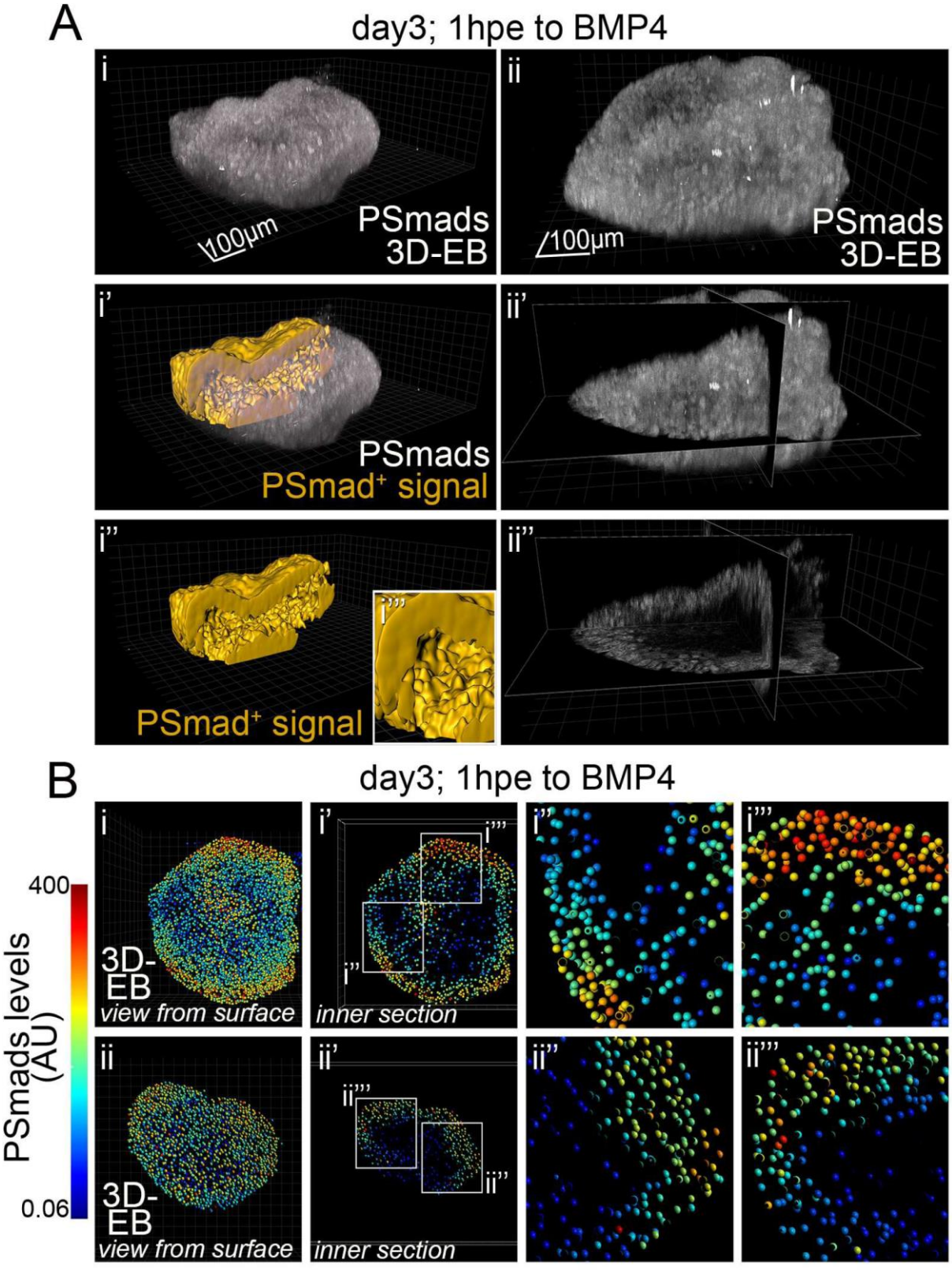

Fig. S4: Spatial restriction of BMP4 mediated Smads activation observed in whole EB

(A) (i,ii) 3D-Reconstruction of whole EB stained for PSmads. **(i'-i''')** Surfaces (in yellow) delimitating PSmads^{+} cells in an EB cut in half with optic scissors, with ii''' a blow-up showing that inner part of the EB is devoid of PSmad signal. **(ii'-ii'')** Position of 3 section plans throughout an EB and signal detected at the level of these plans. *These images demonstrate that Smads activation was restricted to the periphery of whole EB.* **(B)(i,ii)** View from the surface of all segmented cells of an EB. **(i',ii')** Inner optical sections through the EB showing cells displaying some PSmad signal. **(i'', ii'', i''', ii''')** Blow up on two distinct areas, showing in each case an outer-inner gradient of PSmad levels. Smads activation across the outer epithelium displayed a gradient, whose amplitude varied throughout this epithelium.

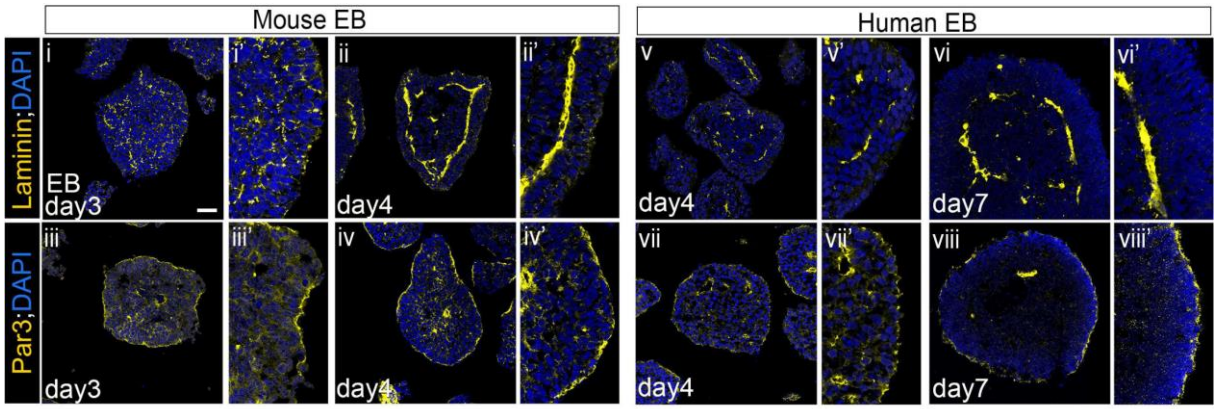

Fig. S5: Par3 and laminin distribution in mouse and human EB during the course of their differentiation

Laminin and Par3 immuno-detection and DAPI labelling in mouse and human EB at the indicated day of differentiation. x' panels are blown up of regions of the x panel (scale bar: 60µM).

Strong Par3 signal delineated the peripheries of the EB and of small lumen inside the EB at all the stages analysed both in human and mouse EB. Laminin was scattered within both mouse and human EB at an early stage of differentiation (day 3 in mouse and day 4 in human), yet it started accumulating and forming a ring separating an outer epithelium from inner epithelia. At later stages of differentiation (day 4 in mouse and day7 in human), this ring was well defined in both species.

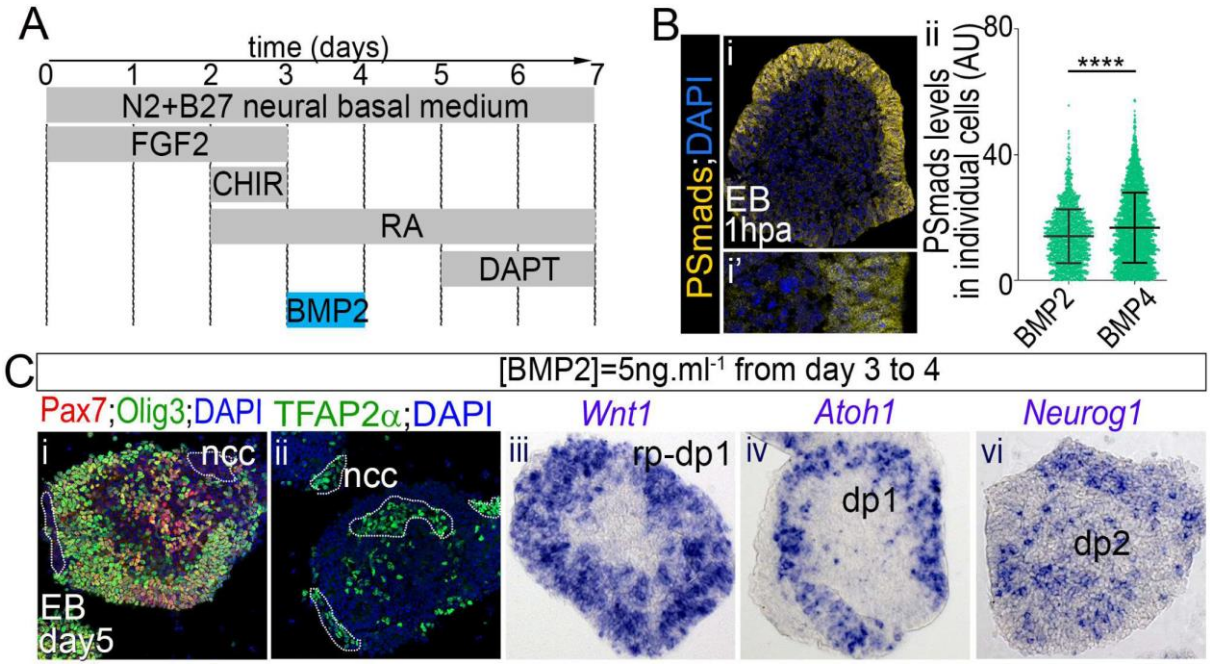

Fig. S6: BMP2 mediated pattern formation

(A) Schematics of the conditions used for the differentiation of the EB shown in Fig. S6. *Note that BMP2 was used instead for BMP4*. **(B)** Immuno-detection of phospho-Smad1/5/9 (PSmads) and DAPI labelling in EB grown 1hour after BMP2 addition to the medium (**i**) and graphs showing the differences between the levels of PSmads in EB cells cultured with BMP2 or BMP4 (**ii**) (mean±s.d., $p<0.0001$). **(C)** Immuno-detection (**i-ii**) and ISH (**iii-vi**) for the indicated NP markers. White dash lines surround ncc territory (scale bar= 60µM).

As observed for BMP4, BMP2 mediated Smads activation was restricted to the outer EB epithelium (Bi). Despite lower levels of Smads activation than measured in presence of BMP4 (Bii), patterns of BMP2 dependent-gene expression were generated in the EB (C), reminiscent to those observed in EB grown with BMP4 (Fig. 1).

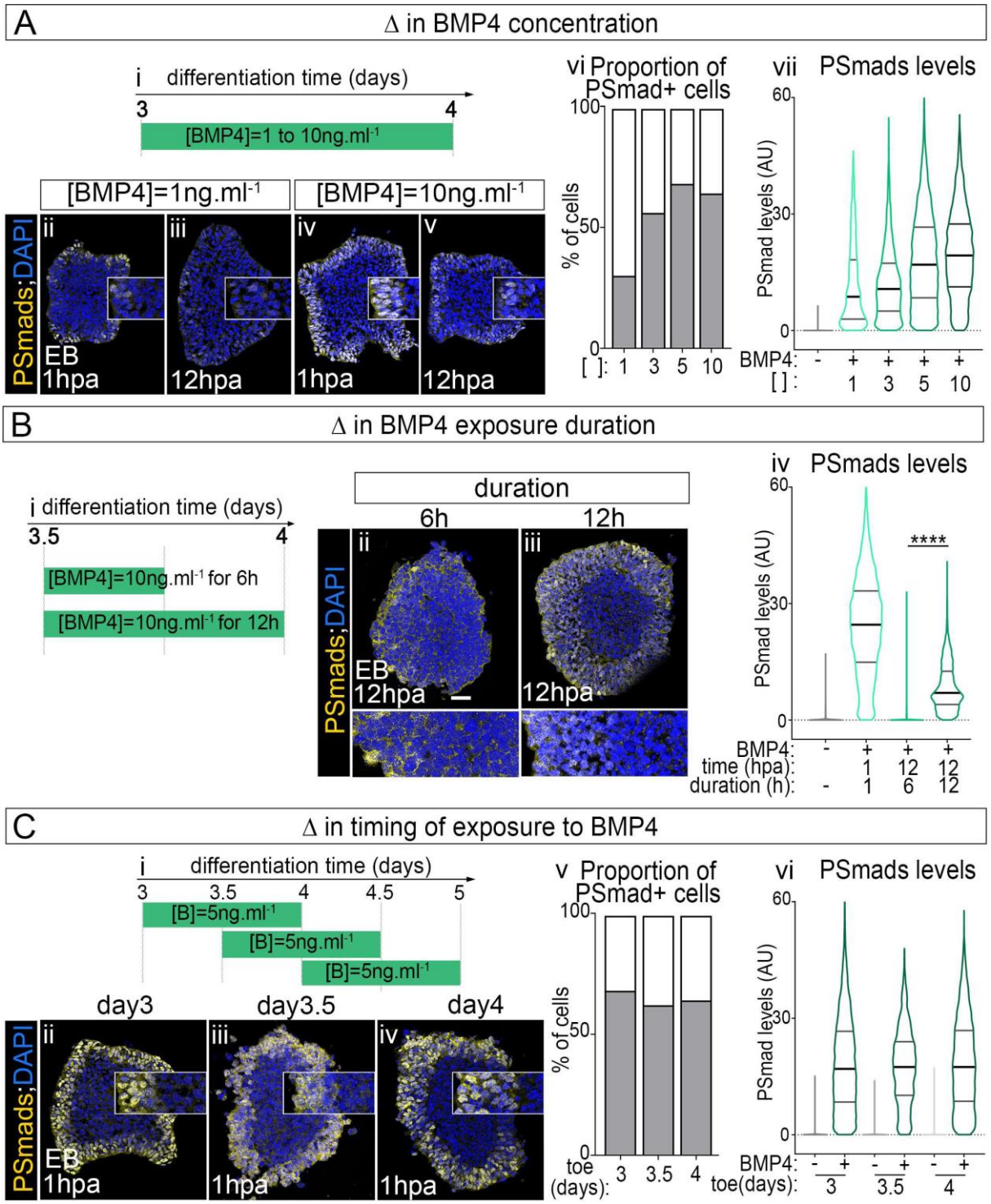

Fig. S7: Effects of BMP4 concentration, exposure duration and timing on Smads activity

Characterization of modulating BMP4 concentration **(A)**, exposure duration **(B)** and timing **(C)** on PSmads levels, spatial distribution and temporal dynamics. **(Ai, Bi, Ci)** Schematics showing BMP4 exposure time windows and concentrations used. **(Aii-v, Bii,iii, Cii-iv)** Immuno-detection of PSmads and DAPI labelling in EB at the indicated time points and conditions (hpa; hour post BMP4 addition). Insets in A and C and lower panels in B are blown ups on PSmads^{+} region. **(Avi, Cv)** Proportion of PSmads^{+} cells per image field. **(Avii, Biv, Cvi)** Violin plots showing PSmads levels in EB cells grown in the indicated conditions.

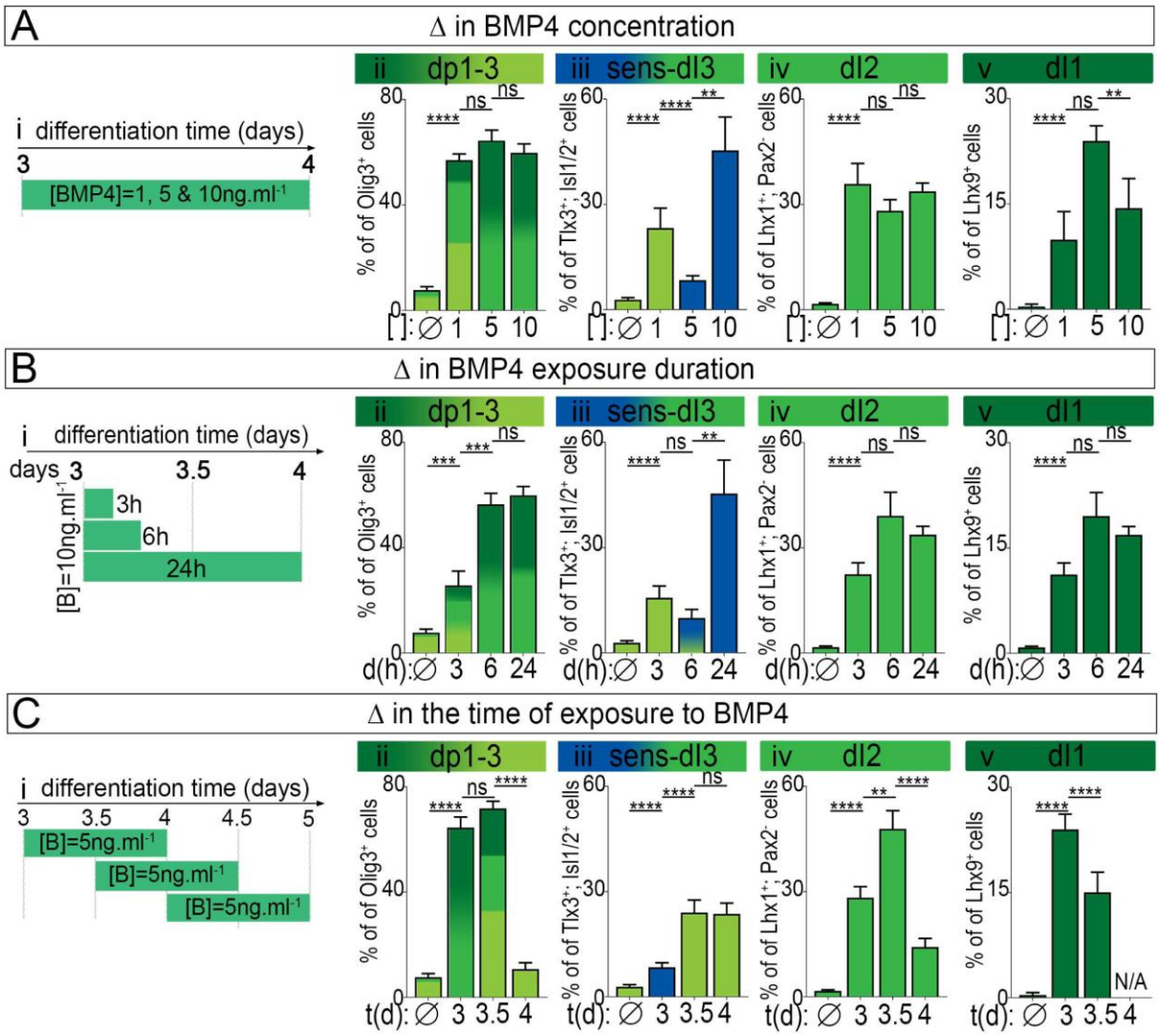

Fig. S8: Effects of BMP4 concentration, exposure timing and duration on the generation of relay IN

Quantifications of the percentage per image field of dp1-dp3 Olig3^{+} NP, dI3, dI2, dI1 and ncc derived sensory cells coloured-coded as in Fig. 1A (circles: individual values, bars: mean±s.e.m.) upon the modulation of BMP4 concentration **(A)**, BMP4 exposure duration **(B)** and the timing of exposure **(C)**. In (**i**), schematics showing the time period and the concentration of BMP4 used. Increasing BMP4 concentration, duration exposure and advancing the time, at which BMP4 was added, promoted the generation of cells with a more dorsal identity.

Table S1. Primer sequences used for qRT-PCR on mouse EB

Fw-*Atoh1*: GCTGGTAAGGAGAAGCGGCTGTG

Rev-*Atoh1*: TGTACCCCATTCACCTGTTTGC

Fw-*Fgf5:* TGTACTGCAGAGTGGGCATC (from (Turner et al., 2017))

Rev-*Fgf5:* ACAATCCCCTGAGACACAGC (from (Turner et al., 2017))

Fw-*Hoxb1:* GGTCAAGAGAAACCCACCTAAG

Rev-*Hoxb1:* CACGGCTCAGGTATTTGTTG

Fw-*Hoxb4*: CACGGTAAACCCCAATTACG

Rev-*Hoxb4*: GAAACTCCTTCTCCAACTCCAG

Fw-*Hoxc6*: ACACAGACCTCAATCGCTCAG

Rev-*Hoxc6*: CGAGTTAGGTAGCGGTTGAAG

Fw-*Id2*: CTCCAAGCTCAAGGAACTGG

Rev-*Id2*: TGCTATCATTCGACATAAGCTCAG

Fw-*Klf4:* GGAAGGGAGAAGACACTGCG

Rev-*Klf4:* ATGTGAGAGAGTTCCTCACGCC

Fw-*Neurog1*: GACACTGAGTCCTGGGGTTC

Rev-*Neurog1*: GTCGTGTGGAGCAGGTCTTT

Fw-*Neurog2*: GTGCAGCGCATCAAGAAGAC

Rev-*Neurog2*: TGAGCGCCCAGATGTAATTG

Fw-*Nkx1.2:* ACTGCCTTCACTTACGAGCA

Rev-*Nkx1.2:* AAATTTTGACCTGCGTCT

Fw-*Pou5f1:* AGTTGGCGTGGAGACTTTGC

Rev- *Pou5f1:* CAGGGCTTTCATGTCCTGG

Fw-*TBP*: GAAGAACAATCCAGACTAGCAGCA

Rev-*TBP*: CCTTATAGGGAACTTCACATCACAG

Table S2. List of antibodies

Antigen	Species	Dilution	Provider (reference)
bHLHE22	Rabbit	1/2500	Abcam (ab204791)
Brachuyry	Goat	1/300	R&D systems (AF2085)
Pou4f1	Mouse	1/400	Chemicon (A5945)
Cdx2	Rabbit	1/1000	Abcam (76541)
Dbx1	Rabbit	1/100	Pierani et al., 1999
FoxD3	Guinea pig	1/5000	From T. Müller and K. Birchmeier (Muller et al., 2005)
Gsx2	Rabbit	1/3000	Millipore (Gsh2, ABN162)
Hoxa5	Rabbit	1/1000	Sigma (HPA029319)
HuC/D	Mouse	1/1000	Thermo Fisher Scientific (16A11)
Islet1/2	Mouse	1/50	DHSB clone 39.4
Laminin	Rabbit	1/500	Sigma (L9393)
Lbx1	Guinea pig	1/10000	From T. Muller and K. Birchmeier
Lhx1/5	Mouse	1/20	DSHB (4F2)
Lhx9	Goat	1/200	Santa Cruz (sc19350 E-14)
Lmx1b	Rabbit	1/10000	From T. Muller and K. Birchmeier
Lmx1b	Guinea pig	1/10000	From T. Muller and K. Birchmeier
Nkx6.1	Mouse	1/50	DSHB (F55A10)
Olig3	Guinea pig	1/10000	From T. Muller and K. Birchmeier
Par3	Rabbit	1/1000	Millipore
Pax2	Rabbit	1/500	Thermo Fisher Scientific (716000)
Pax6	Rabbit	1/250	Biolegend (PRB-278P)
Pax6	Mouse	1/50	DHSB (AB 528427)
Pax7	Mouse	1/50	DSHB (PAX7)
PSmad1/5/9	Rabbit	1/250	Cell Signalling Technology (13820S)
Sox1	Goat	1/200	R&D systems (AF3369)
Sox2	Rabbit	1/200	Thermo Fisher Scientific (48-1400)
Sox9	Goat	1/100	R&D systems (AF3075)
TFAP2α	Rabbit	1/100	Santa Cruz (sc8975)
Tlx3	Rabbit	1/10000	From K. Birchmeier
Secondary antibodies: donkey against mouse, goat, guinea pig or rabbit IgG coupled to Alexa Fluorophores A488, A546, A568 or A647 (Thermo Fisher Scientific) were diluted 1:300 and used with DAPI (500ng/ml, Sigma, 28718-90-3).			

References

Andrews, M. G., del Castillo, L. M., Ochoa-bolton, E., Yamauchi, K., Smogorzewski, J., Butler, S. J., Castillo, L. M., Ochoa-bolton, E., Yamauchi, K., Smogorzewski, J., et al. (2017). BMPs direct sensory interneuron identity in the developing spinal cord using signal-specific not morphogenic activities. *Elife* **6**, 1–24.

Beccari, L., Moris, N., Girgin, M., Turner, D. A., Baillie-Johnson, P., Cossy, A.-C., Lutolf, M. P., Duboule, D. and Arias, A. M. (2018). Multi-axial self-organization properties of mouse embryonic stem cells into gastruloids. *Nature* **562**, 272–276.

Briscoe, J., Pierani, A., Jessell, T. M. and Ericson, J. (2000). A homeodomain protein code specifies progenitor cell identity and neuronal fate in the ventral neural tube. *Cell* **101**, 435–445.

Britz, O., Zhang, J., Grossmann, K. S., Dyck, J., Kim, J. C., Dymecki, S., Gosgnach, S. and Goulding, M. (2015). A genetically defined asymmetry underlies the inhibitory control of flexor–extensor locomotor movements. *Elife* **4**, 1–22.

Dasen, J. S., Tice, B. C., Brenner-Morton, S. and Jessell, T. M. (2005). A Hox regulatory network establishes motor neuron pool identity and target-muscle connectivity. *Cell* **123**, 477–91.

Henrique, D., Abranches, E., Verrier, L. and Storey, K. G. (2015). Neuromesodermal progenitors and the making of the spinal cord. *Development* **142**, 2864–2875.

Hollnagel, A., Oehlmann, V., Heymer, J., Rüther, U. and Nordheim, A. (1999). Id genes are direct targets of bone morphogenetic protein induction in embryonic stem cells. *J. Biol. Chem.* **274**, 19838–45.

Lee, K. J., Dietrich, P. and Jessell, T. M. (2000). Genetic ablation reveals that the roof plate is essential for dorsal interneuron specification. *Nature* **403**, 734–40.

Liu, J. P., Laufer, E. and Jessell, T. M. (2001). Assigning the positional identity of spinal motor neurons: rostrocaudal patterning of Hox-c expression by FGFs, Gdf11, and retinoids. *Neuron* **32**, 997–1012.

Moody, S. A. and LaMantia, A.-S. (2015). Transcriptional Regulation of Cranial Sensory Placode Development. *Curr Top Dev Biol.* **111**, 301–350.

Muller, T., Anlag, K., Wildner, H., Britsch, S., Treier, M., Birchmeier, C. and Müller, T. (2005). The bHLH factor Olig3 coordinates the specification of dorsal neurons in the spinal cord. *Genes Dev* **19**, 733–743.

Pierani, A., Brenner-Morton, S., Chiang, C. and Jessell, T. M. (1999). A Sonic hedgehog-independent, retinoid-activated pathway of neurogenesis in the ventral spinal cord. *Cell* **97**, 903–915.

Samanta, J. and Kessler, J. A. (2004). Interactions between ID and OLIG proteins mediate the inhibitory effects of BMP4 on oligodendroglial differentiation. *Development* **131**, 4131 LP-4142.

Sasai, N., Kutejova, E. and Briscoe, J. (2014). Integration of signals along orthogonal axes of the vertebrate neural tube controls progenitor competence and increases cell diversity. *PLoS Biol.* **12**, e1001907.

Tozer, S., Le Dréau, G., Marti, E., Briscoe, J. and Le Dreau, G. (2013). Temporal control of BMP signalling determines neuronal subtype identity in the dorsal neural tube. *Development* **140**, 1467–74.

Turner, D. A., Girgin, M., Alonso-Crisostomo, L., Trivedi, V., Baillie-Johnson, P., Glodowski, C. R., Hayward, P. C., Collignon, J., Gustavsen, C., Serup, P., et al. (2017). Anteroposterior polarity and elongation in the absence of extra-embryonic tissues and of spatially localised signalling in gastruloids: mammalian embryonic organoids. *Development* **144**,.

Zagorski, M., Tabata, Y., Brandenberg, N., Lutolf, M. P., Tkačik, G., Bollenbach, T., Briscoe, J. and Kicheva, A. (2017). Decoding of position in the developing neural tube from antiparallel morphogen gradients. *Science (80-.).* **356**, 1379–1383.